The Cerebellum (2023) 22:613–627
https://doi.org/10.1007/s12311-022-01429-w

Endothelial Rbpj Is Required for Cerebellar Morphogenesis and Motor Control in the Early Postnatal Mouse Brain

Amelia D. Chapman[1,2] · Samantha Selhorst[1,2] · Julia LaComb[1] · Alexis LeDantec-Boswell[1] · Timothy R. Wohl[1,2] · Subhodip Adhicary[1,3] · Corinne M. Nielsen[1,4,5]

Accepted: 7 June 2022 / Published online: 18 June 2022

Abstract

Intercellular influences are necessary for coordinated development and function of vascular and neural components in the brain. In the early postnatal period after birth, the mammalian cerebellum undergoes extensive morphogenesis — developing its characteristic lobules, organizing its diverse cell types into defined cellular layers, and establishing neural circuits that support cerebellar function, such as coordinated movement. In parallel, the cerebellar vasculature undergoes extensive postnatal growth and maturation, keeping pace with the expanding neural compartment. Endothelial deletion of Rbpj leads to neurovascular abnormalities in mice, including arteriovenous (AV) shunts that supplant capillaries and instead direct high-pressure/high-flow arterial blood directly to veins. Gross and histopathological cerebellar abnormalities, associated with these Rbpj-mediated brain AV malformations (AVMs), led to our hypothesis that early postnatal morphogenesis and lamination of cerebellum was perturbed in mice harboring endothelial Rbpj deficiency from birth. Here, we show that endothelial Rbpj-mutant mice developed enlarged vascular malformations on the cerebellar surface, by 2-week post-Rbpj deletion. In addition, outgrowth of cerebellar lobules was impaired through decreased cell proliferation, but not increased apoptosis, in the external granule layer. Molecular layer thickness was reduced, and the Purkinje layer was affected, by decreased Purkinje cell number, primary dendrite length, and dendritic arbor density. Endothelial deletion of Rbpj also led to impaired motor behaviors, consistent with abnormal cerebellar morphogenesis and lamination. Thus, our data suggest that Rbpj is required, in early postnatal vascular endothelium, to ensure proper cerebellar outgrowth, morphogenesis, and function in mice.

Keywords Cerebellum · Endothelium · Mice · Motor · Neurovascular · Rbpj

Introduction

The mammalian cerebellum is responsible for motor control and higher-order neural function, including cognition. The cerebellum is divided into a series of lobules, each of which is comprised of a stereotypically layered cortex that surrounds an inner core of white matter and cerebellar nuclei. The cerebellar cortex is organized in laminar fashion — the deepest internal granule layer (IGL) is dominated by granule neurons; the middle Purkinje cell layer (PL) consists of Purkinje neurons and Bergmann glia; the more superficial molecular layer (ML) contains numerous cell types and serves as a conduit for parallel fibers and various neuronal terminals; and the most superficial external granular layer (EGL) provides transient residence for progenitor cells that migrate toward the IGL, maturing along the way [1]. Neuronal projections traverse cerebellar layers, with excitatory and inhibitory inputs working in concert to establish proper neuronal circuitry. This laminar organization contributes to circuitry underlying motor functions, such as coordinated movement, motor learning, and body balance [1, 2].

In mice, while cerebellar cell generation and migration are initiated during embryogenesis, many events occur

✉ Corinne M. Nielsen
nielsenc@ohio.edu

1 Department of Biological Sciences, Ohio University, 57 Oxbow Trail, Irvine Hall 107, Athens, OH 45701, USA

2 Honors Tutorial College, Ohio University, Athens, OH 45701, USA

3 Translational Biomedical Sciences Program, Ohio University, Athens, OH 45701, USA

4 Molecular and Cellular Biology Program, Ohio University, Athens, OH 45701, USA

5 Neuroscience Program, Ohio University, Athens, OH 45701, USA

during early postnatal development. Within the first 30 days after birth (postnatal day (P) 1 to P30), whole brain expansion continues, and cerebellar cortex expands 30-fold [3]. During postnatal development, cell layers within the cerebellum likewise experience growth, with peak IGL proliferative capacity and expansion occurring at P8 and P11, respectively, and emergence of the ML at P8 [3]. Development of mouse Purkinje cells occurs largely during the first three postnatal weeks of life, during which Purkinje cells develop dendrites and establish synaptic connections [4]. Thus, PL morphogenesis largely coincides with granule cell proliferation and maturation of GABAergic interneuron precursors in neighboring cerebellar layers [5]. Another aspect of postnatal cerebellar expansion involves proliferation and movement of cells from an inward-to-outward direction. Cells in the EGL, for example, extend outward and permit the expansion of deeper tissue. Anchoring centers, points from which EGL cells proliferate and migrate outwardly, are in position by embryonic day (E) 17.5, and outgrowth from these anchoring centers is a critical step in lobular development [6]. Initial tissue expansion from anchoring centers establishes five primary (or cardinal) lobes by P2. Continued expansion, during a secondary wave of outgrowth and foliation, leads to the mature pattern of ten lobules (folia) in the medial cerebellum (vermis) by P10 and to mature cerebellar size by P28 [6]. These overlapping developmental events that occur in the early postnatal cerebellum rely on intercellular communication — the mechanisms of which are just beginning to be understood.

During early postnatal morphogenetic expansion, the cerebellar vasculature follows similar expansion, with capillary branching and increased vessel number occurring in the emerging PL at P8, in the IGL and PL at P11, and continuing in the ML around P14–15 [3]. Following this inside-out vascularization, mature capillary patterning and density is complete by ~ P30 [3], mirroring the timing of non-vascular tissue expansion described above. While a functional vascular bed is critical to provide nutritional support to brain parenchyma, recent work shows that brain vessels also provide a physical scaffold for migratory neural precursor cells [7–12]. Also, vascular cells — primarily endothelial cells — exert direct influence over developing neural tissue, by secreting paracrine (angiocrine) factors that provide signaling cues for development and maintenance of neural cell types [13–15]. Among known vascular-to-neural influences, those in neurogenic niches, such as embryonic cortical or spinal germinal zones [16, 17] or the postnatal cortical subventricular zone [18–20], are best understood. Given the juxtaposition of neural and vascular cerebellar components, and their parallel expansion in the early postnatal period in mammals, signaling events initiated in vascular endothelium may similarly influence, directly or indirectly, events that govern cerebellar morphogenesis.

The Notch signaling pathway is an evolutionarily conserved, juxtacrine cell signaling mechanism, which is essential in a broad range of tissue types for development and homeostasis [21]. As a downstream transcription factor and effector of canonical Notch, Rbpj (Recombinant signal binding protein for immunoglobulin kappa J region) is critical for propagating Notch signaling [22]. Genetic studies in mice have revealed that Notch-Rbpj signaling is required in vascular endothelium to regulate vascular development, remodeling, and maintenance, in embryonic, early postnatal, and adult blood vessels [23–27]. We previously reported the development of vascular abnormalities — brain arteriovenous (AV) malformations (AVMs) — in mice, following endothelial deletion of Rbpj, at birth [26]. Clinically, this human neurovascular disease is characterized by direct AV shunting and nidus formation, both of which disrupt healthy brain vasculature and hemodynamics. Using this early postnatal, endothelial Rbpj-deficient genetic mouse model, we identified abnormalities in postnatal cerebellar vascular and lobular morphogenesis, including effects on neuronal layers — EGL, ML, PL — and corresponding behavioral deficits. Our findings indicate that Rbpj is required in early postnatal endothelium to ensure proper postnatal development of the mammalian cerebellum.

Methods

Mice

Mouse lines, *Cdh5(PAC)-CreERT2* [28], *Rbpsuh* (*Rbpj*)^{flox} [29], and *Rosa26*$^{mT/mG}$ [30], were provided by Taconic Biosciences (Breeding Agreement 13,073), Dr. Tasuku Honjo (Kyoto University, Japan), and Dr. Liqun Luo (Stanford University School of Medicine, Stanford, CA, USA), respectively. On postnatal day (P) 1 and P2, 100 µg Tamoxifen (TAM) (Sigma) in 50 µl peanut oil (Planters) was injected intragastrically into both control and mutant pups [26]. PCR-based genotyping was performed to identify control versus mutant pups, as previously described [26]. Male and female mice were used indiscriminately. For motor tests, data were analyzed for all mice (both biological sexes included) (Fig. 5) and for separate female and male cohorts (Supplementary Fig. 9). All experiments were performed in accordance with Ohio University IACUC approved Animal Protocol 16-H-024.

Tissue Harvest and Preparation

Prior to tissue harvest, mice were anesthetized, perfused via inferior vena cava with DyLight488-conjugated *Lycopersicon esculentum* (tomato) lectin (Vector Labs), then transcardially perfused with 1% paraformaldehyde (PFA). Brain tissue was then removed from the skull and immersion fixed in 4% PFA overnight, at 4 °C, with gentle agitation. Post-fixation, tissue was rinsed in phosphate-buffered saline (PBS). Whole brains were imaged for cerebellum measurements, by covering brain with PBS, in a 1.5% agarose-bottomed dish. An agarose divot permitted angling of brain for imaging. Light microscopy images were acquired with a Nikon SMZ745 microscope and Nikon NIS Elements software. Next, brains were hemisected and processed for paraffin infiltration/embedding or 30% sucrose infiltration/cryoembedding, following standard techniques [26]. Paraffin tissue blocks were stored at room temperature and frozen tissue blocks were stored at − 80 °C, prior to sectioning. For vascular imaging, the cerebellum was dissected from the brain, and cerebellar hemispheres were removed. With the remaining vermis tissue, a micro-scalpel was used to trim off the outermost ~ 2 mm of the vermis surface, without damaging the most superficial tissue. Next, the vermis was placed in a PBS-filled parafilm well, affixed to a microscope slide. A coverslip was applied to gently flatten the vermis between microscope slide and coverslip for fluorescent confocal imaging.

Histological Staining

Mid-sagittal, 6 µm thick paraffin sections were collected, using a rotary microtome (AO Spencer). Sections were stained with hematoxylin and eosin, according to standard protocol [31]. Light microscopy images were acquired, using a dissection microscope (Nikon SMZ745) or upright microscope (Nikon NiU) and Nikon NIS Elements software.

Immunostaining, EdU (5-Ethynyl-2′-deoxyuridine) Incorporation, and TUNEL (Terminal Deoxynucleotidyl Transferase dUTP Nick End Labeling) Detection

For immunofluorescence, mid-sagittal, 12 µm thick cryosections were collected, using a cryostat (Leica). Following brief post-fixation (4% PFA) and rinsing (PBS), tissue sections were blocked in 5% donkey serum/0.1% Triton-X/PBS and incubated with appropriate antibodies. Primary antibodies were anti-Calbindin D28K (1:2000) (Swant) and anti-NeuN (1:1000) (Sigma). Secondary antibodies were Cy3 donkey-anti-mouse (1:500) (Jackson ImmunoResearch). For anti-Calbindin labeling only, (1) tris-buffered saline was used for rinses; and (2) signal amplification was performed — tissue was incubated in biotinylated donkey-anti-mouse (1:500) (Jackson ImmunoResearch), then Alexa647-streptavidin (1:500) (Jackson ImmunoResearch). For immunohistochemistry, mid-sagittal, 6 µm thick paraffin sections were collected, using a rotary microtome (AO Spencer). Tissue was deparaffinized in xylenes and rehydrated, prior to antigen retrieval in sub-boiling sodium citrate. Primary anti-RBPSUH (clone D10A4) antibody (Cell Signaling Technology) was diluted 1:100 in diluent from manufacturer. Boost Detection Reagent (Cell Signaling Technology) was used according to manufacturer's instructions. DAB reagent (Sigma) was used for chromogen deposition. Cell nuclei were counterstained with hematoxylin. For EdU (Invitrogen) incorporation, mice received intraperitoneal injection of 10 µg EdU/g body weight on P12, P13, and P14; tissue was harvested (per above) at + 2 h on P14. Detection of incorporated EdU followed manufacturer's instructions, using Click-iT™ Plus labeling/detection reaction with AlexaFluor® 647 component (Invitrogen). Detection of TUNEL + nuclei followed manufacturer's instructions, using Click-iT™ Plus TUNEL reaction with AlexaFluor® 647 component (Invitrogen). Nuclei in all tissue sections were stained with DAPI (4',6-diamidino-2-phenylindole) (Invitrogen), mounted onto slides with ProLong Gold™ (Invitrogen), and coverslipped for imaging. Fluorescent and bright-field microscopy images were acquired with a Nikon NiU microscope and NIS Elements software.

Confocal Imaging

Confocal Z-stacks were acquired, ranging from 16 to 40 slices, at 2 µm steps, using a Zeiss LSM 510 laser scanning confocal microscope system. Z-stacks were projected at maximum intensity.

Behavioral Testing

All behavioral testing was performed in accordance with Ohio University IACUC approved animal protocol 16-H-024. Methods followed those previously reported [32]. Motor testing was performed on P14 male and female mice. (1) Ambulation: we constructed a 22-inch long by 4-inch-wide runway apparatus, with 6-inch-high walls and no top, out of clear plexiglass; a lengthwise insert permitted adjusting the corridor width down to 2 inches. A black box was positioned at the end of the corridor, as incentive. For the testing period, a mouse was placed in the corridor and monitored/recorded, at side view, for forward movement (ambulation) via crawling or walking, with or without symmetry. Two minutes of ambulation was assessed and scored as 0 = no movement, 1 = crawling with asymmetric limb movement, 2 = slow crawling but symmetric limb movement, and 3 = fast crawling/walking. (2) Hindlimb angle:

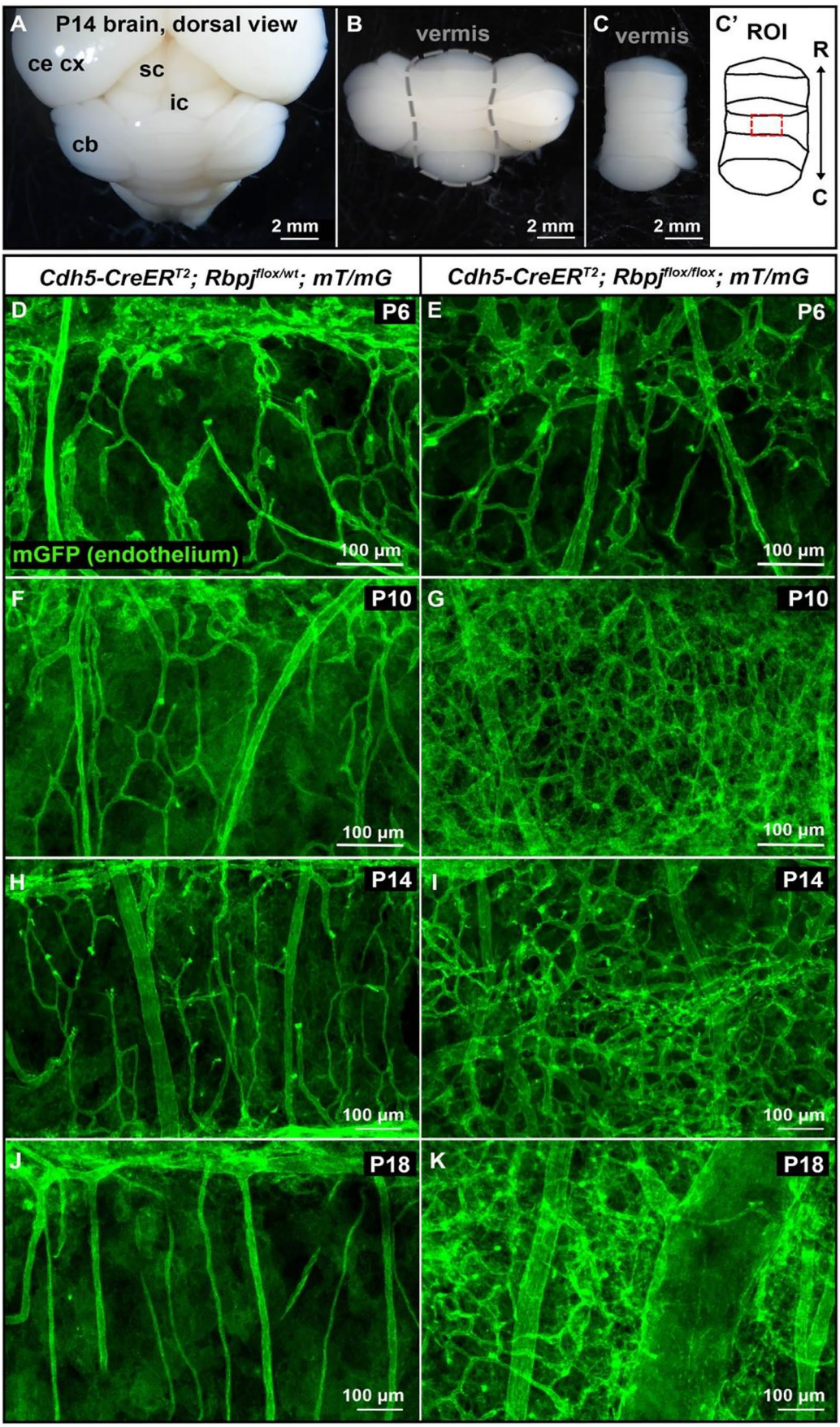
A P14 brain, dorsal view
ce cx
sc
ic
cb
2 mm
B vermis
2 mm
C vermis
2 mm
C' ROI
R
C
Cdh5-CreER^{T2}; Rbpj$^{flox/wt}$; mT/mG
Cdh5-CreER^{T2}; Rbpj$^{flox/flox}$; mT/mG
D P6
mGFP (endothelium)
100 µm
E P6
100 µm
F P10
100 µm
G P10
100 µm
H P14
100 µm
I P14
100 µm
J P18
100 µm
K P18
100 µm

◂**Fig. 1** Enlarged and disorganized vasculature was present from P10 to P18 in cerebellum, following endothelial deletion of Rbpj. **A**–**C** Steps in microdissection to isolate intact vermis from whole P14 cerebellum. **C'** Approximate region of interest (ROI) of vermis shown in **D**–**K**, along the rostral-caudal (R–C) axis. **D**–**K** Whole mount confocal imaging of cerebellar vasculature, with endothelial cells highlighted by mGFP, from the *Rosa26*$^{mT/mG}$ allele. **D**–**E** At P6, surface cerebellum vessels appeared similar in control and mutant brains. **F**–**K** Rbpj$^{i\Delta EC}$ mutant vessels were visibly enlarged and disorganized from P10 to P18, as compared to controls. For each timepoint, $N=3$ controls and $N=3$ mutants. Cerebral cortex (ce cx); superior colliculi (sc); inferior colliculi (ic); cerebellum (cb); spinal cord (sp cd)

mouse movement down our custom corridor was recorded/monitored, at birds-eye view. Hindlimb angle was assessed and measured by pausing video during ambulation and drawing a straight line from heel to tip of middle digit, for each hindlimb. Lines were extended to intersection point, and the resulting angle was measured. (3) Grasping reflex: pup was gently scruffed, and mouse paw was stroked over the blunt, rounded edge of a protectively covered razor blade — a straight edge safe and narrow enough for neonatal mouse grasping. Front- and hind-paws were tested and scored, individually, for ability or inability to grasp blade edge. (4) Negative geotaxis: we constructed a 45° slope, using cardboard box lid lined with absorbent lab bench pad — the pad offered traction and gripping surface for mouse paws. Mice were placed, face pointing down the slope, and gently held in position for 5 s. After release, the time lapsed to turn its body was measured.

Data Presentation and Statistical Analysis

Figures were prepared using Adobe Creative Cloud Photoshop software. Statistical tests were completed with GraphPad Prism software. Control vs. mutant values were compared, using Student's *t*-test with Welch's correction. For each motor test, three trials were scored/measured and averaged. All error bars indicate standard deviation. Statistical significance was reported as $*P<0.05$, $**P<0.01$, $***P<0.001$, and $****P<0.0001$.

Results

Enlarged and Disorganized Vasculature Was Present in P10 to P18 Cerebellum, Following Endothelial Deletion of Rbpj

To overcome vascular imaging limitations caused by the inherent foliation of postnatal cerebellum, we used a microdissection technique to remove the superficial-most ~ 2 mm of vermis tissue (Fig. 1A–C), from *Cdh5(PAC)-CreER*^{T2}*; Rbpj*$^{flox/wt}$ (control) and *Cdh5(PAC)-CreER*^{T2}*; Rbpj*$^{flox/flox}$ (Rbpj$^{i\Delta EC}$ or mutant) mice (genetic manipulation described in [26] and schematized in Supplementary Fig. 1B). Effective deletion of Rbpj from endothelial cells lining cerebellar vessels was verified at P7, following ligand-inducible excision of *Rbpj* exons 6–7 from P1, P2 (Supplementary Fig. 1C–D). These data corroborated previous findings showing Rbpj deficiency from (i) cerebellar endothelial cells (ECs) 6 weeks-post deletion in adult mice and (ii) cortical ECs 14 days-post deletion in neonatal mice [26]. While increased endothelial density was previously reported in thin cryosections through P14 cerebellum, following endothelial deletion of Rbpj from birth [26], a whole mount view of abnormal cerebellar vasculature was not reported. To image cerebellar blood vessels, we genetically labelled vascular endothelium, using the *Rosa26*$^{mT/mG}$ Cre-responsive reporter allele, in control (*Cdh5(PAC)-CreER*^{T2}*; Rbpj*$^{flox/wt}$*; Rosa26*$^{mT/mG}$) and Rbpj$^{i\Delta EC}$ mutant (*Cdh5(PAC)-CreER*^{T2}*; Rbpj*$^{flox/flox}$*; Rosa26*$^{mT/mG}$) mice. To understand the time course of early postnatal vascular morphogenesis in the cerebellum, we harvested mice in 4-day intervals at P6, P10, P14, and P18. Confocal imaging of mGFP-positive ECs permitted visualization of cerebellar vermis vascular architecture, as situated on the cerebellar surface. At P6, there were no apparent differences between control and mutant cerebellum vessels (Fig. 1D–E). However, at P10, P14, and P18, Rbpj$^{i\Delta EC}$ cerebellum vessels appeared enlarged and disorganized, resembling an unrefined vascular plexus, as compared to controls (Fig. 1F–K). While direct AV connections could not be identified in either control (capillaries) or mutant (AV shunts), our findings corroborate previous bead assay data, which demonstrated that 15-µm-diameter beads lodged in capillaries of control cerebellum but bypassed AV shunts in Rbpj$^{i\Delta EC}$ mutants [26]. These findings are consistent with vascular abnormalities previously described in P14 frontal cortex, following endothelial Rbpj deletion from birth [26], and suggest that endothelial Rbpj is required for vascular morphogenesis in the early postnatal cerebellum.

Endothelial Deletion of Rbpj Impaired Cerebellum Morphogenesis, Including Outgrowth from Anchoring Centers

To investigate cerebellum morphogenesis, we analyzed cerebellar areas and growth axes from whole brain images of control and Rbpj$^{i\Delta EC}$ mice, harvested at P6, P10, P14, and P18. This temporal analysis allowed us to measure consequences to cerebellar growth over time, in the context of advancing vascular malformation pathologies. To assess overall postnatal cerebellar growth, following endothelial deletion of Rbpj from birth, we first measured tracings of whole cerebellar and vermis areas (dorsal view) from control and mutant mice. Both whole cerebellar area and vermis area were significantly reduced in mutant brain by P14 and P18, but not by P6 or P10, as compared to controls (P14

Fig. 2A–E; P18 Supplementary Fig. 4A–B, F–G; P6 Supplementary Fig. 2A–B, F–G; P10 Supplementary Fig. 3A–B, F–G). To understand cerebellar growth axes that may be affected in our mutant mice, we next measured rostral-caudal length, medial–lateral length, and rostral-caudal:medial–lateral ratio from whole cerebellum (dorsal view). Both rostral-caudal and medial–lateral axial lengths were decreased in mutant cerebellum by P14 and P18, but not by P6 or P10, as compared to controls (P14 Fig. 2B–C, F–G; P18 Supplementary Fig. 4C–D; P6 Supplementary Fig. 2C–D; P10 Supplementary Fig. 3C–D), suggesting impaired growth along cerebellar axes, following endothelial deletion of Rbpj. In addition, the ratio of rostral-caudal to medial–lateral length was decreased in P14 and P19 (but not P6 or P10) mutant cerebellum (P14 Fig. 2H; P18 Supplementary Fig. 4E; P16 Supplementary Fig. 2E; P10 Supplementary Fig. 3E), suggesting that endothelial Rbpj deficiency may affect growth along the rostral-caudal axis more severely than growth along the medial–lateral axis.

To assess morphogenetic outgrowth, specifically, we analyzed anchoring center placement, cerebellar area, and lobule outgrowth, using sagittal, H&E-stained sections through control and mutant brain tissue. We first traced cerebellar perimeter from sagittal sections and overlayed representative control and mutant tracings. Notably, anchoring centers aligned from control and mutant tracings, indicating proper

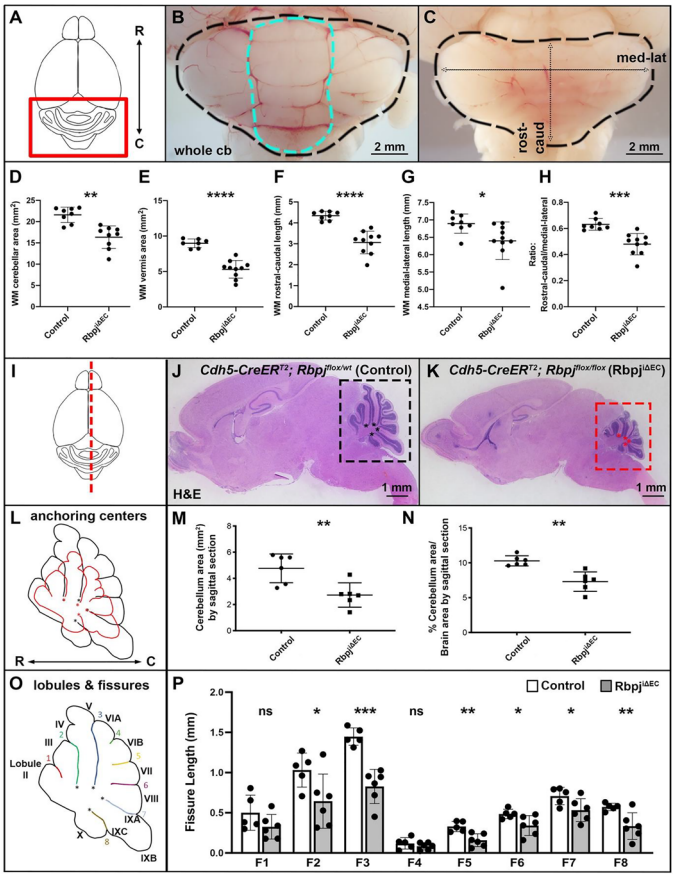

Fig. 2 Endothelial deletion of Rbpj impaired cerebellum morphogenesis, including outgrowth from anchoring centers. **A** Schematic of mouse brain with cerebellum region boxed. Rostral-caudal (R–C) axis is shown. **B**–**C** Control and Rbpj$^{i\Delta EC}$ cerebellum, with cerebellar area (black outline), vermis area (gray outline), rostral-caudal length, and medial–lateral length indicated. Abnormalities in mutant cerebellum (C) were evident by gross morphology. **D**–**H** Images from whole mount (WM) cerebellum were used to measure cerebellar area ($P=0.0016$) and vermis area ($P<0.0001$), rostral-caudal ($P<0.0001$) and medial–lateral ($P=0.0435$) lengths, and the ratio of rostral-caudal/medial–lateral lengths ($P=0.0002$) were decreased in Rbpj$^{i\Delta EC}$ mice, as compared to controls. **I** Schematic indicates plane of mid-sagittal section. **J**–**K** Histologically stained sections through control and Rbpj$^{i\Delta EC}$ brain. Boxes indicate cerebellum; asterisks indicate primary anchoring centers. **L** Outlines of control (black) and Rbpj$^{i\Delta EC}$ (red) cerebellum are overlayed, with anchoring centers aligned. Rostral-caudal (R–C) axis is shown. **M**–**N** Cerebellum area ($P=0.0063$) and proportion of cerebellum area/whole brain area ($P=0.0019$), as measured from mid-sagittal sections, was decreased in Rbpj$^{i\Delta EC}$ mice, as compared to controls. **O** Schematic indicates cerebellum lobules (Roman numerals), fissures (Arabic numerals), and anchoring centers (asterisks). **P** Select fissures were decreased in length in Rbpj$^{i\Delta EC}$ mice, as compared to controls. Fissure (F)2 ($P=0.0289$); F3 ($P=0.0003$); F5 ($P=0.0010$); F6 ($P=0.0242$); F7 ($P=0.0307$); F8 ($P=0.0094$)

anchoring center placement in Rbpj$^{i\Delta EC}$ cerebellum at all timepoints analyzed (P14 Fig. 2I–L; P6 Supplementary Fig. 2H; P10 Supplementary Fig. 3H; P18 Supplementary Fig. 4H). We next used perimeter tracings to measure cerebellar area. While no differences were found at P6 or P10, we noted a downward trend in cerebellum area by P10. By P14 to P18, sagittal cerebellum area was decreased in mutant mice, as compared to controls (P14 Fig. 2M; P6 Supplementary Fig. 2I; P10 Supplementary Fig. 3I; P18 Supplementary Fig. 4I). Because overall body weight is decreased by P14 (but not by P7) in Rbpj$^{i\Delta EC}$ mice [26], we sought to control for potential differences in total brain size between controls and mutants. We calculated the percentage of sagittal brain area occupied by cerebellum and found decreased cerebellum/brain area in mutants by P14 and P18, a decreasing trend by P10, and no change by P6, as compared to controls (P14 Fig. 2N; P6 Supplementary Fig. 2 J; P10 Supplementary Fig. 3J; P18 Supplementary Fig. 4 J). As postnatal cerebellum morphogenesis includes outgrowth from anchoring centers and stereotyped formation of lobules, we measured fissure length as an indicator of cerebellar outgrowth. For analysis, fissures were numbered from mid-sagittal sections through vermis, as shown in Fig. 2O. Because not all cerebellar lobules are present in every mid-sagittal section — for example, lobule I was rarely seen — the eight fissures represent those extending from primary anchoring centers and those extending from a secondary wave of foliation. By P6, no fissures were reduced in length (Supplementary Fig. 2 K); by P10, P14, and P18, fissures were consistently reduced in length in Rbpj$^{i\Delta EC}$ cerebellum (P14 Fig. 2P; P10 Supplementary Fig. 3 K; P18 Supplementary Fig. 4 K). Notably, both fissures emanating from anchoring centers (fissures 2, 3, 7, 8) and fissures emanating during a secondary wave of lobulation (fissures 4, 5, 6) were consistently affected from ~ P10 to P18 in Rbpj$^{i\Delta EC}$ mutants. Together, these data suggest that endothelial Rbpj deficiency impaired lobule outgrowth from anchoring centers and led to a disproportionately smaller cerebellum.

Endothelial Deletion of Rbpj Disrupted Stereotypical Cerebellar Lamination

Postnatal lobule outgrowth involves proliferation and migration of progenitor cells within the EGL, with the EGL reaching peak proliferative capacity at P8 [3]; thus, we reasoned that the EGL may be affected in Rbpj$^{i\Delta EC}$ mutants. Given that the EGL extends from anchoring centers, lines fissures, and extends around the lobule (H&E-stained tissue showed cells in EGL between two lobules, Fig. 3B–C), we measured EGL thickness (defined as DAPI-stained nuclei in the EGL) and cell proliferation at proximal (within fissures) and distal (lobule tips) aspects (regions shown in Fig. 3A). Given that lobulation continues along a postnatal timeline, with different lobules extending outward at different developmental timepoints, we analyzed the EGL lobule-by-lobule. We measured EGL thickness using DAPI-stained sections (Fig. 3D–E) and found decreased proximal or distal EGL thickness by P14, in select cerebellum lobules (Fig. 3F–G). We next measured EdU incorporation within the EGL as an indicator of cell proliferation. We injected EdU at P12, 13, 14 and harvested brain tissue at 2 h post-injection on P14; thus, we analyzed EdU incorporation events spanning P12–14 in the EGL (Fig. 3D–E). We found decreased proportion of EdU + cells in the EGL of Rbpj$^{i\Delta EC}$ mutants (reported in Fig. 3H as percent EdU + /DAPI + nuclei per EdU − /DAPI + nuclei), suggesting fewer proliferative EGL cells, following endothelial deletion of Rbpj (representative images of each cerebellar lobule shown in Supplementary Fig. 5A–AB). Notably, in 0/6 controls and 4/6 mutants, EGL fusions — in partial spans of the EGL — were noted between adjacent cerebellar lobules (corresponding to proximal aspect of lobules) (Supplementary Fig. 6A–C). EGL fusions were not included in EGL thickness measurements, as cells in EGL fusions could not be assigned clearly to one lobule or its adjacent neighbor. To assess for apoptosis in the EGL, we performed TUNEL staining and found no evidence for TUNEL + cells in the EGL of P14 control or mutant cerebellum (Supplementary Fig. 6D–E). These data suggest that loss of endothelial Rbpj impaired EGL cell proliferation without increased apoptosis or altered EGL thickness.

As proliferative granule cell progenitors in the EGL produce postmitotic neurons and neural precursors that dive inward to populate the IGL, we hypothesized that cell density and/or granule cell number in the IGL may be affected in Rbpj$^{i\Delta EC}$ cerebellum. For cell density, we counted the number of IGL nuclei per lobule area and found no significant difference in IGL cell density — except for lobule VII — in P14 Rbpj$^{i\Delta EC}$ cerebellum, as compared to controls (Supplementary Fig. 7A–D). Immunostaining against NeuN, a marker for postmitotic neurons, showed similar neuronal density in the IGL of P14 control and Rbpj$^{i\Delta E}$ cerebellum (Supplementary Fig. 7E–F). However, given that both cerebellar outgrowth and proliferation of granule neuron progenitors were decreased by P14, we reasoned that the total number of granule neurons in the IGL would be decreased. We counted NeuN + nuclei in cerebellum lobule VII (a representative lobule consistently affected in Rbpj$^{i\Delta E}$ cerebellum) and found fewer NeuN + IGL cells in P14 mutants (Supplementary Fig. 7E'–G). Thus, while IGL cell density was not affected, the number of IGL cells (at least in representative lobule VII) were fewer in number, following endothelial deletion of Rbpj. These results are consistent with a role for endothelial Rbpj in influencing cerebellum tissue expansion.

Given that cells actively migrate into and through the cerebellar molecular layer, during their movement from EGL to

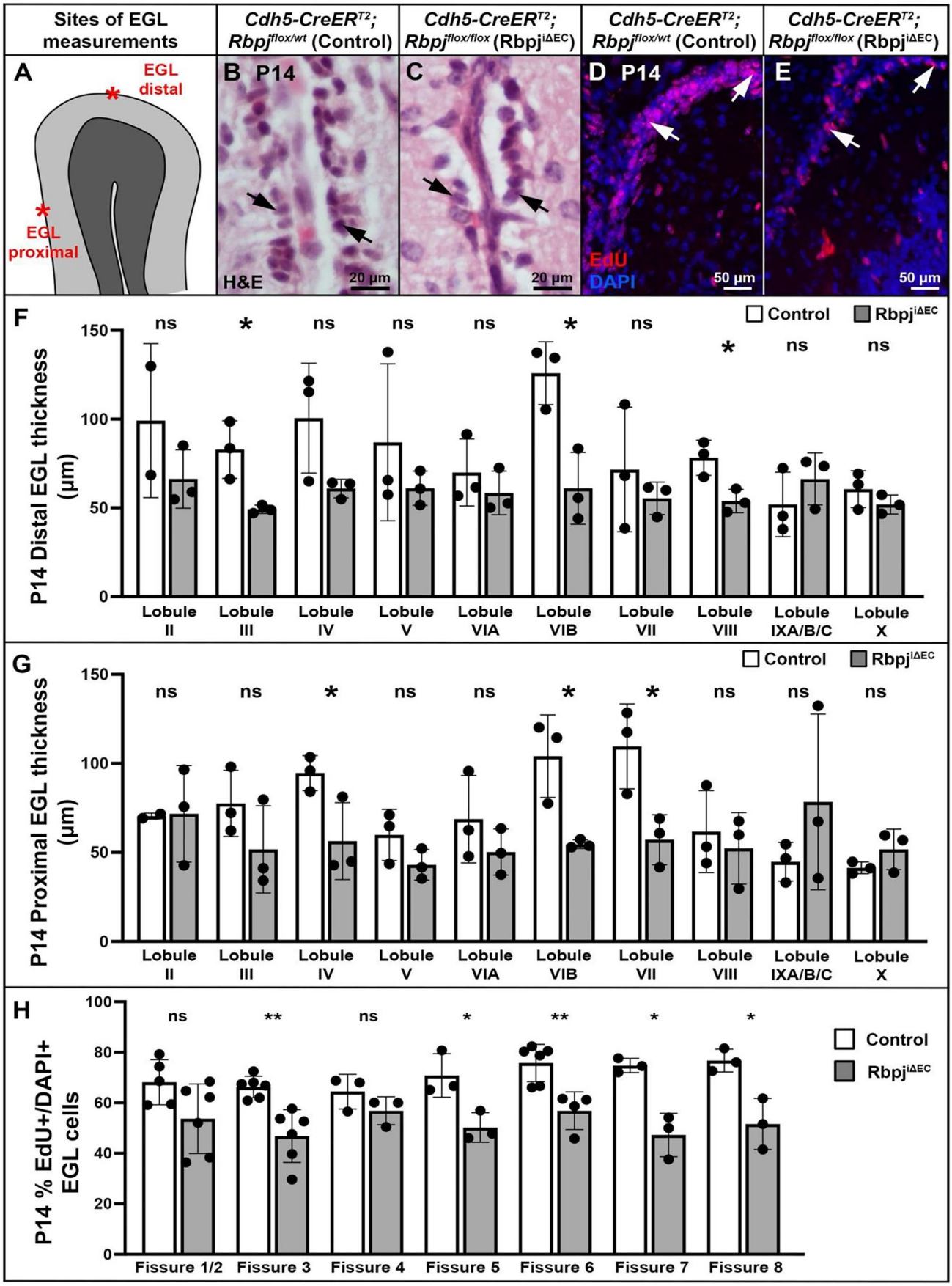
Sites of EGL measurements
Cdh5-CreER^T2; Rbpj^flox/wt (Control)
Cdh5-CreER^T2; Rbpj^flox/flox (RbpjiΔEC)
Cdh5-CreER^T2; Rbpj^flox/wt (Control)
Cdh5-CreER^T2; Rbpj^flox/flox (RbpjiΔEC)
A
EGL distal
EGL proximal
B P14
H&E
20 μm
C
20 μm
D P14
EdU
DAPI
50 μm
E
50 μm
F
Control
RbpjiΔEC
P14 Distal EGL thickness (μm)
ns * ns ns ns * ns * ns ns
Lobule II
Lobule III
Lobule IV
Lobule V
Lobule VIA
Lobule VIB
Lobule VII
Lobule VIII
Lobule IXA/B/C
Lobule X
G
Control
RbpjiΔEC
P14 Proximal EGL thickness (μm)
ns ns * ns ns * * ns ns ns
Lobule II
Lobule III
Lobule IV
Lobule V
Lobule VIA
Lobule VIB
Lobule VII
Lobule VIII
Lobule IXA/B/C
Lobule X
H
P14 % EdU+/DAPI+ EGL cells
ns ** ns * ** * *
Control
RbpjiΔEC
Fissure 1/2
Fissure 3
Fissure 4
Fissure 5
Fissure 6
Fissure 7
Fissure 8

◂**Fig. 3** Endothelial deletion of Rbpj disrupted cell proliferation in the external granule layer. **A** Schematic of cerebellum lobule shows two sites (proximal and distal) for measuring EGL (external granule layer) thickness. **B–C** Histologically stained mid-sagittal sections through P14 control and Rbpj$^{i\Delta EC}$ cerebellum. Arrows indicate proximal EGLs from two adjacent lobules. **D–E** EdU nuclear incorporation (from P12 to P14) (red) and DAPI counterstain (blue) in P14 control and Rbpj$^{i\Delta EC}$ cerebellum. **F** Distal EGL thickness was measured and quantified. EGL thickness was decreased in select lobules in mutant, as compared to controls. Lobule (Lob) III ($P=0.0234$); Lob VIB ($P=0.0145$); Lob VIII ($P=0.0233$). **G** Proximal EGL thickness was measured and quantified. EGL thickness was decreased in select lobules in mutant, as compared to controls. Lob IV ($P=0.0494$); Lob VIB ($P=0.0214$); Lob VII ($P=0.0304$). **H** Proportions of EdU + nuclei per DAPI + nuclei in the EGL were quantified. Fissure (F)3 ($P=0.0045$); F5 ($P=0.0326$); F6 ($P=0.0064$); F7 ($P=0.0225$); F8 ($P=0.0338$)

IGL, and given morphological changes previously noted, we measured molecular layer thickness in control and Rbpj$^{i\Delta EC}$ cerebellum. We measured molecular layer thickness (using histologically stained tissue) (Fig. 4A–C), at both proximal and distal aspects, of each cerebellar lobule. By P14, molecular layer thickness was consistently and severely decreased in every lobule, except lobule X, in Rbpj$^{i\Delta EC}$ cerebellum, as compared to controls. Molecular layer thickness was decreased around the perimeter of each affected lobule, as measured at both proximal and distal aspects (Fig. 4D–E). In P10 Rbpj$^{i\Delta EC}$ cerebellum, only lobule IV, distal molecular layer thickness, was significantly decreased (Supplementary Fig. 8A–B). These data suggest that the molecular layer was increasingly affected, over postnatal time, during the Rbpj$^{i\Delta EC}$-mediated cerebellar pathogenesis.

We next analyzed possible effects on Purkinje neurons, whose cell bodies comprise the cerebellar Purkinje laminar layer, and whose characteristic dendritic arbors reside in the molecular layer. To examine Purkinje neuron number, we immunostained against Calbindin and counted the number of Calbindin + Purkinje neurons per field of cerebellum tissue (reported as cell number per 1 mm^2 tissue), in mid-sagittal sections through each cerebellar lobule. While Purkinje neurons properly aligned in both control and Rbpj$^{i\Delta EC}$ cerebellum, the number of Purkinje neurons in Rbpj$^{i\Delta EC}$ cerebellum was significantly decreased in lobules III through VII and lobules IV through VIII, by P10 and P14, respectively, as compared to controls (P10 Supplementary Fig. 8C, F–G; P14 Fig. 4F–H). Purkinje neurons extend elaborate dendritic arbors into the cerebellar molecular layer. Given the diminished molecular layer in Rbpj$^{i\Delta EC}$ cerebellum, we reasoned that Purkinje dendritic arbors would be affected, either being reduced in size or crowded into the narrowed molecular layer. To assess effects on Purkinje neuron dendrites, we first traced and measured the primary dendrites of Calbindin + Purkinje neurons. We found decreased primary dendrite length at P14, in Rbpj$^{i\Delta EC}$ cerebellum, as compared to controls (Fig. 4I) but not at P10 (though a downward trend was noted) (Supplementary Fig. 8D). We analyzed the density of Calbindin + dendritic arbors by determining the percentage of Calbindin + area per molecular layer area. We found reduced dendritic arbor density in P10 and P14 Rbpj$^{i\Delta EC}$ cerebellum, as compared to controls (P10 Supplementary Fig. 8E; P14 Fig. 4J). Together, these data suggest that endothelial Rbpj deficiency, during early postnatal development, impaired branching and growth of cerebellar Purkinje dendrites.

Endothelial Rbpj Deficiency Impaired Motor Behaviors in Mice

Given the morphogenetic and laminar abnormalities consequences to early postnatal cerebellum — in particular, vermis — development, following endothelial Rbpj deletion from birth, we reasoned that motor behaviors would be affected in Rbpj$^{i\Delta EC}$ mice. We evaluated motor behaviors using a series of tests specifically designed to measure gait stability, motor coordination, and fine motor movement, in neonatal/early postnatal mice, aged P3–P15 [32]. We first analyzed ambulation — the forward motion, walking gait pattern — of control and mutant P14 mice. Mice received an ambulation score, based on the degree of forward motion observed in three trials: 0 = no forward motion; 1 = crawling with asymmetric limb movement; 2 = slow crawling with symmetric limb movement; 3 = fast/continuous crawling/walking. Consistently, Rbpj$^{i\Delta EC}$ mice received lower ambulation score, as compared to controls (Fig. 5A). During the ambulation test, Rbpj$^{i\Delta EC}$ mice appeared to ambulate with splayed limbs and paws; thus, we performed a hindlimb angle test, by measuring the angle at which hind-paws were placed during ambulation. Indeed, Rbpj$^{i\Delta EC}$ mice placed hind-paws splayed outward, as evidenced by increased hindlimb angle, compared to controls (Fig. 5B). We next tested front- and hind-paw grasping reflex, in control and mutant P14 mice. At this early postnatal age, the test for grasping reflex is designed to test the ability to grasp and not a fear-induced grasp response (reported to develop post-P15) [32]. Grasping ability was assessed in front- and hind-paws, by assigning one point per paw; thus, a trial with a score of "3" means three of four paws showed ability to grasp. Results from three trials per mouse were averaged, and Rbpj$^{i\Delta EC}$ mice scored significantly lower on the grasping reflex test, as compared to controls (Fig. 5C). To test innate, neonatal responses to vestibular and motor cues, we performed a negative geotaxis test. We measured the elapsed time to turn face-up, after being placed in a face-down position on a 45° slope, and we found no significant difference in Rbpj$^{i\Delta EC}$ vs. controls (Fig. 5D).

To control for and identify potential differences among biological sexes, we re-analyzed our motor behavior datasets among separate P14 male and female cohorts. Both

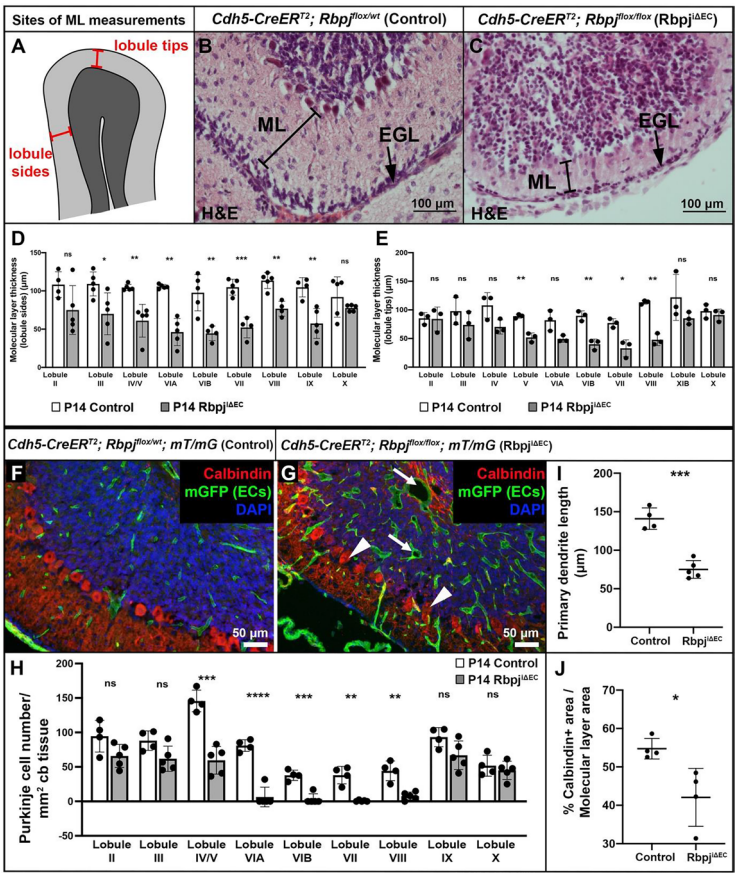

Fig. 4 Endothelial Rbpj deficiency affected molecular layer thickness, Purkinje cell number, and dendritic density. **A** Schematic of cerebellum lobule shows two sites (tips and sides) for measuring ML (molecular layer) thickness. **B**–**C** Histologically stained mid-sagittal sections through P14 control and Rbpj$^{i\Delta EC}$ cerebellum. Bracket indicates measurement for ML thickness. Quantified in **D**. Lobule (Lob) III ($P=0.0301$); Lob IV/V ($P=0.0096$); Lob VIA ($P=0.0015$); Lob VIB ($P=0.0047$); Lob VII ($P=0.0009$); Lob VIII ($P=0.0010$); Lob IX ($P=0.0033$) and in **E** Lob V ($P=0.0064$); Lob VIB ($P=0.0024$); Lob VII ($P=0.0192$); Lob VIII ($P=0.0042$). **F**–**G** Immunostaining against Calbindin, to label Purkinje neurons (red) in P14 control and Rbpj$^{i\Delta EC}$ cerebellum. mGFP + endothelial cells (ECs) are green, DAPI + nuclei are blue. Arrows indicate abnormally enlarged blood vessel; arrowheads indicate Purkinje neuron cell bodies. **H** Quantification of Calbindin + Purkinje cell number per mm^2 tissue, by lobule, in P14 control and Rbpj$^{i\Delta EC}$ cerebellum. Lob IV/V ($P=0.0002$); Lob VIA ($P<0.0001$); Lob VIB ($P=0.0003$); Lob VII ($P=0.0095$); Lob VIII ($P=0.0098$). **I** Average length of primary Purkinje neuron dendrites was decreased in P14 Rbpj$^{i\Delta EC}$, as compared to controls ($P=0.0003$). **J** Purkinje neuron dendritic arbor density, as measured by %Calbindin + area of the molecular layer, was decreased in P14 Rbpj$^{i\Delta EC}$, as compared to controls ($P=0.0375$)

female and male cohorts of Rbpj$^{i\Delta EC}$ mutant mice received lower ambulation scores (Supplementary Fig. 9A–A') and showed larger hindlimb angle splay (Supplementary Fig. 9B–B') than controls. On the grip test, female mutant mice received significantly lower grasping reflex scores than female controls, and male mutant mice received downward-trending scores, as compared to male controls (Supplementary Fig. 9C–C'). Neither male nor female cohorts showed differences in the negative geotaxis test, in Rbpj$^{i\Delta EC}$ mutants vs. controls (Supplementary Fig. 9D–D'). Taken together, data from the early postnatal behavioral tests suggest impaired motor control in mutant mice, as compared to controls. Such neurological deficits are consistent with abnormal morphological and laminar development, and subsequent consequences to cerebellar motor circuitry, without confounding deficits to vestibular function.

Discussion

Formation of Rbpj-mediated vascular malformations, during the early postnatal period, coincides with cerebellar growth and morphogenesis. In Rbpj$^{i\Delta EC}$ cerebellum, postnatal vascular development is perturbed, leading to enlarged and disorganized vasculature. In cerebellum tissue, initial morphogenetic patterning events, such as establishment of anchoring points and formation of cardinal lobes, which occur prior to P3, proceeded normally. However, morphogenetic events, including lobule outgrowth and lamination,

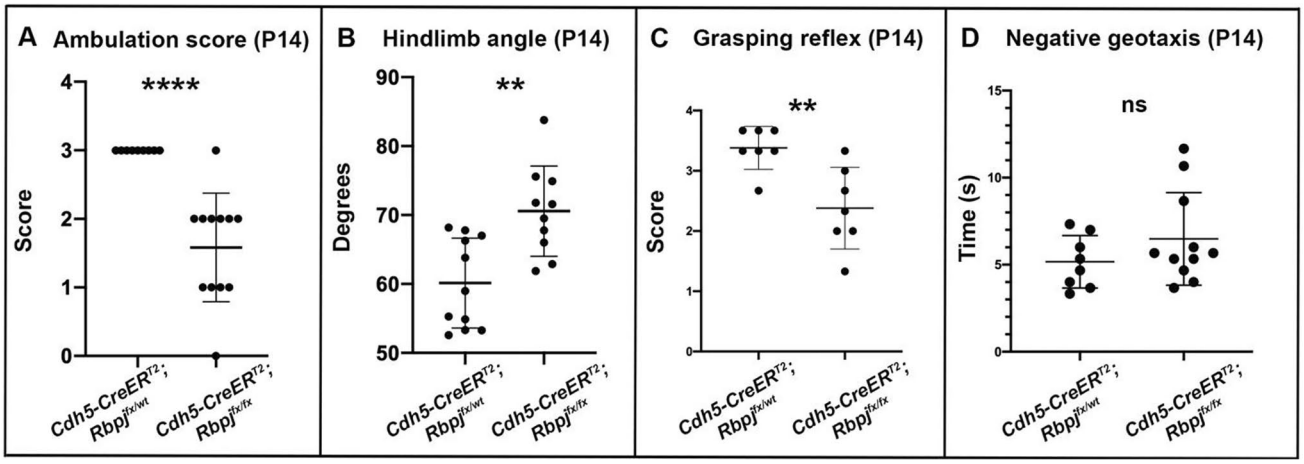

Fig. 5 Endothelial Rbpj deficiency, from birth, impaired motor behaviors in mice by P14. Neonatal-specific motor tests were performed on male and female mice. Analyses included data grouped from both biological sexes. **A** P14 mutant mice received lower ambulation scores than controls. $N=9$ controls and $N=12$ mutants, 3 trials each. $P<0.0001$. **B** P14 mutant mice showed larger hindlimb angle splay than controls. $N=11$ controls and $N=10$ mutants, 3 measurements each, averaged. $P=0.0017$. **C** P14 mutant mice received lower grasping reflex score than controls. $N=7$ controls and $N=7$ mutants, 3 trials each, averaged. $P=0.0048$. **D** Time for P14 mutant mice to turn body from nose-down to nose-up, on 45° incline, did not differ from controls. $N=8$ controls and $N=11$ mutants, 3 trials each, averaged. $P=0.1896$

which occur after P3, were affected. These data suggest that early postnatal endothelial Rbpj is critical for cerebellum vascular development and for a secondary wave of lobulation and rapid cerebellar expansion.

Endothelial Rbpj Is Necessary for Proper Vascular Organization in the Early Postnatal Cerebellum

Our time course study of whole-mount cerebellum vasculature uncovered vessel malformations as early as P10 and persistent through P18, the last timepoint examined (fewer than 10% of Rbpj$^{i\Delta EC}$ mice survive to P21) [26]. These vascular abnormalities were severe by P10, a timepoint at which cerebellum outgrowth problems were just beginning to trend and/or manifest. These results suggest that intact endothelial Rbpj, from intact cerebellum vasculature, influences cerebellum tissue growth.

Endothelial Rbpj Is Required for Postnatal Cerebellum Morphogenesis, Including Outgrowth from Anchoring Centers

Our findings indicate that intact endothelial Rbpj is required for proper cerebellar size during early postnatal morphogenesis in mice. While the placement of fixed anchoring centers was not affected by endothelial deficiency of Rbpj, both fissure length and cerebellum area were affected, suggesting a defect in outgrowth of lobules from the anchoring centers. It has been shown that granule cell precursors (GCPs) — resident cells of the EGL — are proliferative during foliation and outgrowth, and the shape of GCPs also changes as they push outward toward the lobule tips [6]. Further, GCP proliferation is regulated by Sonic hedgehog (Shh) signaling, initiated by Shh secretion from Purkinje cells; thus, postnatal cerebellum expansion and foliation requires Shh-mediated GCP expansion and production of granule cells [33, 34]. Our data suggest that stunted lobule outgrowth in the endothelial Rbpj-deficient mice resulted, at least in part, from decreased GCP proliferation and/or directed movement from the base of cerebellar fissures toward the tips of the outward-growing lobules. We noted EGL fusions in 67% of mutant cerebella, which may have impaired GCP movement and morphological changes that are required for lobule outgrowth. After the central lobe forms from the anchoring centers, a second wave of lobulation generates non-principal fissures to form lobules VIA-VIII [6, 35]. Thus, lobulation and outward growth of lobules VIA-VIII are secondary to outward growth that is initiated from the anchoring centers. Consistently, we found abnormalities in lobules VIA-VIII, which correspond to tissue outgrowth formed in the secondary wave of lobulation and which may extend from yet-undescribed "secondary anchoring centers" (refer to Fig. 6). Because these lobules are preferentially affected in endothelial Rbpj-deficient cerebellum, this suggests that endothelial Rbpj may regulate a secondary wave of lobule and fissure morphogenesis, in the postnatal cerebellum.

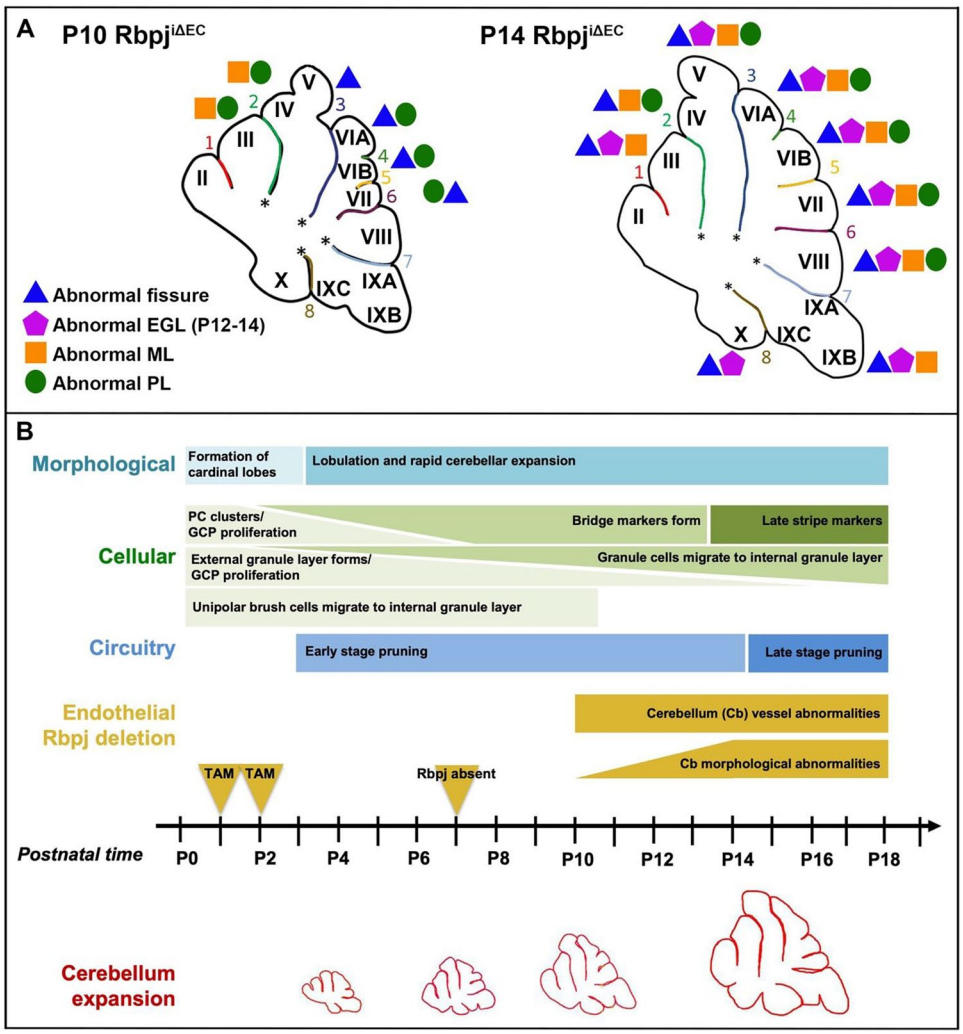

Fig. 6 Summary of cerebellar lobules with abnormalities at P10 and P14, following endothelial deletion of Rbpj from birth. **A** Summary of consequences to cerebellum by P10 (left) and P14 (right), in mutant mice, as compared to controls. Asterisks = primary anchoring centers; Arabic numerals = fissures; Roman numerals = lobules. **B** Early postnatal timeline of cerebellar developmental events, aligned with experimental design and findings from this study. Adapted from [1]. Following Tamoxifen (TAM) administration at P1 and P2, endothelial Rbpj protein was absent by P7. Vascular abnormalities and consequences to cerebellum morphogenesis were observed from P10 to P18

Endothelial Rbpj Is Required for Proper Neuronal Lamination in Early Postnatal Cerebellum

Endothelial Rbpj deficiency, in the early postnatal period of cerebellar development, affected select stereotypical, laminar neuronal layers. Molecular later thickness was reduced in most lobules by P14; notably, lobules that form during the secondary foliation were preferentially affected, consistent with the timing of Rbpj deficiency. Our analysis of the IGL showed that cellular density was not significantly affected in Rbpj-mutant mice, but that fewer NeuN + neurons were present in the IGL. Fewer IGL granule neurons could result from the impaired proliferation of GCPs in the mutant EGL and/or from impaired granule cell migration to the IGL. Our data suggest that impaired GCP proliferation is responsible, at least in part, for the decreased number of cells within the mutant IGL; thus, endothelial Rbpj is required to influence GCP proliferation and ultimately IGL cell number in the early postnatal cerebellum. Finally, endothelial Rbpj deletion affected Purkinje neuron number and morphology, with dendritic arbors severely stunted in outgrowth and density. These data are consistent with reduced molecular layer data, as Purkinje neuron dendritic arbors reside in the molecular layer and may influence, or be influences by, molecular layer thickness. As discussed above, Shh secretion by Purkinje neurons regulates GCP proliferation in the EGL and thus cerebellum outgrowth and foliation [33, 34]. Loss of Purkinje cells predictably decreases Shh secretion and GCP proliferation in the EGL. Thus, the role for endothelial Rbpj to promote healthy Purkinje cell numbers likely disrupts Shh signaling and cellular proliferation in GCPs residing in the EGL. Alternatively, loss of Purkinje neurons may be attributed to necrotic cell death, as generation and migration of Purkinje neurons preceded Rbpj manipulation [5] and as we found no evidence for neuronal apoptosis. Overall, our results indicate that endothelial Rbpj is required in the early postnatal period for proper cerebellar lamination.

Rbpj Is Required in Early Postnatal Endothelium for Proper Motor Function

The cerebellum is involved in motor coordination/movement, and lesions to the cerebellar vermis have been associated with altered gait patterns in human patients [36]. Our data indicate that the cerebellum, notably the vermis, was severely affected following endothelial deletion of Rbpj. Thus, the impaired movement observed in P14 mice, following endothelial deletion of Rbpj, may result — either directly or indirectly — from impaired motor circuit function. Supporting this possibility, motor deficits in Rbpj-mutant mice are consistent with Purkinje neuron abnormalities. At birth, Purkinje neurons are innervated by numerous climbing fiber projection neurons; within 3 weeks, successive refinement of neuronal connections ensures just one climbing fiber innervates one Purkinje neuron [37]. In our Rbpj-deficient mice, impaired movement (reported in [26]) could result from overall ill health of mutant mice or from vestibular defects, as opposed to motor deficits elicited by abnormal cerebellar circuitry. Our battery of motor tests was reported to test neurological function, including motor reflexes, versus select fear responses and vestibular defects [32]. Our data analyses by biological sex revealed that differences in motor behavior between control and $Rbpj^{i\Delta EC}$ mutant mice were consistent, when datasets were separated into female and male cohorts. Though a significant difference in grasping reflex was not seen among control and mutant males, the data showed a clear downward trend with perhaps one mutant male outlier. Finally, while we cannot rule out all other skeletomuscular defects that could impair animal movement, our data suggest direct motor impairments related to impaired cerebellum development following loss of endothelial Rbpj.

Abnormal gait has been reported in patients suffering from vascular diseases, such as peripheral artery disease [38], cerebral small vessel disease [39], or brain AVM [40]. In such cases, motor deficit is predicted to result from impaired or hemorrhagic blood flow to brain tissue. While our data cannot definitively answer whether (1) endothelial Rbpj is required to ensure a healthy cerebellar vasculature and thus support circuitry formation, or (2) endothelial Rbpj influences neural components to develop properly and establish functional motor circuits, our results nonetheless indicate that Rbpj is required in early postnatal endothelium to support motor function.

Do Varying Phenotypes at P10 and P14 in Rbpj-Deficient Mice Reflect Differential Regulation by Endothelial Rbpj or Brain AVM Progression?

Select features of postnatal cerebellar development were affected as early as P10 following endothelial Rbpj deletion from birth. While overall cerebellar area was not significantly altered by P6 or P10, fissure length — primarily of secondary lobules — was selectively decreased. Molecular layer thickness was not affected by P10; however, ML thickness was reduced by P14. Given the emergence of ML at P8 [3], and its later-emerging vascular expansion, this suggests a later-stage (post-P11) requirement for endothelial Rbpj in the ML. Purkinje neurons were affected by P10, including decreased cell number and diminished dendritic arbor area (but not decreased primary dendrite length), suggesting an earlier requirement for endothelial Rbpj in Purkinje layer development. Regarding the vascular phenotype, whole vessel malformations and impaired vascular organization were observed as early as P10 and continued through P18; however, vascular abnormalities were not observed as early as P6, suggesting that the vascular phenotype was initiated between ~ P7 and P9. These data are consistent with vascular malformation data from $Rbpj^{i\Delta EC}$ frontal cortex that showed phenotypic onset by P8, through P14 [26]. Our new findings indicate that cerebellar morphogenetic abnormalities advance in parallel with vascular abnormalities. However, it remains unknown whether cerebellar defects result from temporally different regulation by endothelial Rbpj or from consequences of progressive vascular impairment.

Direct vs. Indirect Consequences of Endothelial Rbpj Deficiency to Postnatal Cerebellar Development

In addition to their critical role in nutrient delivery, blood vessels also secrete angiocrine factors that regulate a variety of cellular processes. Angiocrine roles for endothelial Notch signaling, including hematopoietic stem cell support, osteoclast function, and cardiomyocyte growth, have been described [20, 22]. Identification of molecules secreted by endothelial cells, from distinct vascular beds, will help determine whether vascular-to-neural influences, such as those regulated by Notch/Rbpj, are direct or indirect. In the brain, intercellular influences are indeed critical for brain growth and health. Capillary-level blood vessels (microvessels) comprise part of a unique anatomical and functional unit, called the neurovascular unit (NVU). The NVU includes multiple distinct vascular (endothelial cells, pericytes) and neural (astrocytes, neurons, microglia) cell types, which reside in close apposition to one another — for example, astrocytic endfeet contact microvessel endothelial cells [41]. Collectively, the NVU ensures proper neurovascular development and function within the brain. Understanding how specific intercellular signaling events are involved in the developing cerebellum will aid our understanding of direct versus indirect cell–cell influences, to ensure neurovascular health and function.

The Cerebellum Is Uniquely and Preferentially Affected in Select Neurovascular Diseases

Cerebellar AVMs fall into a specialized class of brain AVM, according to the established clinical classification system, in part because their foliated anatomy [42]. For example, the broadly used Spetzler-Martin grading system, which applies standardized measures to predict and recommend AVM treatment responses, is not a consistently accurate clinical tool for cerebellar AVMs [42]. Rather, a supplementary system was developed to predict treatment outcomes for cerebellar AVMs, which are more likely to present with hemorrhage and neurological deficits, than cerebral AVMs [42]. Our Rbpj mouse model may represent a useful tool for studying features and pathogenic mechanisms of cerebellar AVM formation that impact cerebellar development and function.

Supplementary Information

Supplementary Information The online version contains supplementary material available at https://doi.org/10.1007/s12311-022-01429-w.

Acknowledgements We thank Kayleigh Fanelli for assistance with confocal imaging; Ohio University IACUC and Laboratory for Animal Research for animal care; Ohio University Histopathology Core for access to cryostat; and Ohio University Neuroscience Program for access to confocal microscope.

Author Contribution A.D.C. and C.M.N. conceptualized and designed experiments; A.D.C., S.S., J.L., A.L.-B., T.R.W., S.A., and C.M.N. performed experiments and analyzed data; and A.D.C. and C.M.N. wrote the manuscript.

Funding This research was supported by Ohio University Honors Tutorial College Research Apprenticeship to A.D.C.; Ohio University Summer Neuroscience Undergraduate Research Fellowships to A.L.-B., S.S., and T.R.W.; and start-up funding from Ohio University College of Arts & Sciences to C.M.N.

Declarations

Competing Interests The authors declare no competing interests.

References

1. White JJ, Sillitoe RV. Development of the cerebellum: from gene expression patterns to circuit maps: Development of cerebellum. Wiley Interdiscip Rev Dev Biol. 2013;2:149–64.
2. Ito M. Historical review of the significance of the cerebellum and the role of Purkinje cells in motor learning. Ann N Y Acad Sci. 2002;978:273–88.
3. Acker T, Beck H, Plate KH. Cell type specific expression of vascular endothelial growth factor and angiopoietin-1 and -2 suggests an important role of astrocytes in cerebellar vascularization. Mech Dev. 2001;108:45–57.
4. Sotelo C, Dusart I. Intrinsic versus extrinsic determinants during the development of Purkinje cell dendrites. Neuroscience. 2009;162:589–600.
5. Dusart I, Flamant F. Profound morphological and functional changes of rodent Purkinje cells between the first and the second postnatal weeks: a metamorphosis? Front Neuroanat [Internet]. 2012 [cited 2021 Dec 15];6. Available from: http://journal.frontiersin.org/article/https://doi.org/10.3389/fnana.2012.00011/abstract
6. Sudarov A, Joyner AL. Cerebellum morphogenesis: the foliation pattern is orchestrated by multi-cellular anchoring centers. Neural Develop. 2007;2:26.
7. Snapyan M, Lemasson M, Brill MS, Blais M, Massouh M, Ninkovic J, et al. Vasculature guides migrating neuronal precursors in the adult mammalian forebrain via brain-derived neurotrophic factor signaling. J Neurosci. 2009;29:4172–88.
8. Won C, Lin Z, Kumar TP, Li S, Ding L, Elkhal A, et al. Autonomous vascular networks synchronize GABA neuron migration in the embryonic forebrain. Nat Commun. 2013;4:2149.
9. Xi Y, Chen WJ, Deng JX, Cui ZJ, Liu HL, Yan MC, et al. Vasculature-guided neural migration in mouse cerebellum. Ital J Zool. 2015;82:15–24.
10. Paredes MF, James D, Gil-Perotin S, Kim H, Cotter JA, Ng C, et al. Extensive migration of young neurons into the infant human frontal lobe. Science. 2016;354:aaf7073.
11. Tsai H-H, Niu J, Munji R, Davalos D, Chang J, Zhang H, et al. Oligodendrocyte precursors migrate along vasculature in the developing nervous system. Science. 2016;351:379–84.
12. Tan X, Liu WA, Zhang X-J, Shi W, Ren S-Q, Li Z, et al. Vascular influence on ventral telencephalic progenitors and neocortical interneuron production. Dev Cell. 2016;36:624–38.
13. Daneman R, Zhou L, Agalliu D, Cahoy JD, Kaushal A, Barres BA. The mouse blood-brain barrier transcriptome: a new resource for understanding the development and function of brain endothelial cells. Ikezu T, editor. PLoS ONE. 2010;5:e13741.
14. Bjornsson CS, Apostolopoulou M, Tian Y, Temple S. It takes a village: constructing the neurogenic niche. Dev Cell. 2015;32:435–46.
15. Paredes I, Himmels P, Ruiz de Almodóvar C. Neurovascular communication during CNS development. Dev Cell. 2018;45:10–32.
16. Javaherian A, Kriegstein A. A stem cell niche for intermediate progenitor cells of the embryonic cortex. Cereb Cortex. 2009;19:i70–7.
17. Li S, Haigh K, Haigh JJ, Vasudevan A. Endothelial VEGF sculpts cortical cytoarchitecture. J Neurosci. 2013;33:14809–15.
18. Ottone C, Krusche B, Whitby A, Clements M, Quadrato G, Pitulescu ME, et al. Direct cell–cell contact with the vascular niche maintains quiescent neural stem cells. Nat Cell Biol. 2014;16:1045–56.
19. Licht T, Keshet E. The vascular niche in adult neurogenesis. Mech Dev. 2015;138:56–62.
20. Ramasamy SK, Kusumbe AP, Adams RH. Regulation of tissue morphogenesis by endothelial cell-derived signals. Trends Cell Biol. 2015;25:148–57.
21. Borggrefe T, Oswald F. The Notch signaling pathway: transcriptional regulation at Notch target genes. Cell Mol Life Sci. 2009;66:1631–46.
22. Fernández-Chacón M, García-González I, Mühleder S, Benedito R. Role of Notch in endothelial biology. Angiogenesis. 2021;24:237–50.

23. Krebs LT, Xue Y, Norton CR, Shutter JR, Maguire M, Sundberg JP, et al. Notch signaling is essential for vascular morphogenesis in mice. Genes Dev. 2000;14:1343–52.
24. Krebs LT, Shutter JR, Tanigaki K, Honjo T, Stark KL, Gridley T. Haploinsufficient lethality and formation of arteriovenous malformations in Notch pathway mutants. Genes Dev. 2004;18:2469–73.
25. Copeland JN, Feng Y, Neradugomma NK, Fields PE, Vivian JL. Notch signaling regulates remodeling and vessel diameter in the extraembryonic yolk sac. BMC Dev Biol. 2011;11:12.
26. Nielsen CM, Cuervo H, Ding VW, Kong Y, Huang EJ, Wang RA. Deletion of Rbpj from postnatal endothelium leads to abnormal arteriovenous shunting in mice. Development. 2014;141:3782–92.
27. Cuervo H, Nielsen CM, Simonetto DA, Ferrell L, Shah VH, Wang RA. Endothelial notch signaling is essential to prevent hepatic vascular malformations in mice: Notch signaling prevents hepatic vascular malformations in mice. Hepatology. 2016;64:1302–16.
28. Sörensen I, Adams RH, Gossler A. DLL1-mediated Notch activation regulates endothelial identity in mouse fetal arteries. Blood. 2009;113:5680–8.
29. Tanigaki K, Han H, Yamamoto N, Tashiro K, Ikegawa M, Kuroda K, et al. Notch–RBP-J signaling is involved in cell fate determination of marginal zone B cells. Nat Immunol. 2002;3:443–50.
30. Muzumdar MD, Tasic B, Miyamichi K, Li L, Luo L. A global double-fluorescent Cre reporter mouse. Genesis. 2007;45:593–605.
31. Hassell J, Hand AR. Tissue fixation with diimidoesters as an alternative to aldehydes I. Comparison of cross-linking and ultrastructure obtained with dimethylsuberimidate and glutaraldehyde. J Histochem Cytochem. 1974;22:223–39.
32. Feather-Schussler DN, Ferguson TS. A battery of motor tests in a neonatal mouse model of cerebral palsy. J Vis Exp. 2016;53569.
33. Corrales JD, Blaess S, Mahoney EM, Joyner AL. The level of sonic hedgehog signaling regulates the complexity of cerebellar foliation. Development. 2006;133:1811–21.
34. Wechsler-Reya RJ, Scott MP. Control of neuronal precursor proliferation in the cerebellum by sonic hedgehog. Neuron. 1999;22:103–14.
35. Sillitoe RV, Joyner AL. Morphology, molecular codes, and circuitry produce the three-dimensional complexity of the cerebellum. Annu Rev Cell Dev Biol. 2007;23:549–77.
36. Ilg W, Giese MA, Gizewski ER, Schoch B, Timmann D. The influence of focal cerebellar lesions on the control and adaptation of gait. Brain. 2008;131:2913–27.
37. Carrillo J, Nishiyama N, Nishiyama H. Dendritic translocation establishes the winner in cerebellar climbing fiber synapse elimination. J Neurosci. 2013;33:7641–53.
38. Szymczak M, Krupa P, Oszkinis G, Majchrzycki M. Gait pattern in patients with peripheral artery disease. BMC Geriatr. 2018;18:52.
39. de Laat KF, van Norden AGW, Gons RAR, van Oudheusden LJB, van Uden IWM, Bloem BR, et al. Gait in elderly with cerebral small vessel disease. Stroke. 2010;41:1652–8.
40. Krauss JK, Kiriyanthan GD, Borremans JJ. Cerebral arteriovenous malformations and movement disorders. Clin Neurol Neurosurg. 1999;101:92–9.
41. Sweeney MD, Ayyadurai S, Zlokovic BV. Pericytes of the neurovascular unit: key functions and signaling pathways. Nat Neurosci. 2016;19:771–83.
42. University of California. San Francisco Arteriovenous Malformation Study Project, Rodríguez-Hernández A, Kim H, Pourmohamad T, Young WL. Lawton MT Cerebellar arteriovenous malformations Neurosurgery. 2012;71:1111–24.